Structure and characteristics of C_3N_4 thin films prepared by rf plasma-enhanced chemical vapor deposition

Wu Dawei, Fu Dejun, Guo Huaixi, Zhang Zhihong, Meng Xianquan, and Fan Xiangjun
Ion Beam Physics Laboratory, Department of Physics, Wuhan University, Wuhan 430072, People's Republic of China
(Received 18 October 1996; revised manuscript received 15 January 1997)

C_3N_4 films were prepared on Si(111) by rf plasma-enhanced chemical vapor deposition using Si_3N_4/TiN and Si_3N_4/ZrN as transition layers. X-ray diffraction and transmission electron diffraction revealed that the films deposited have a polycrystalline structure. X-ray photoelectron spectroscopy (XPS) and Fourier transform infrared spectroscopy confirmed the presence of sp^3 and sp^2 hybridized C atoms tetrahedrally and hexagonally bonded with N atoms, respectively. The nitrogen concentration was calculated from the XPS spectra. Graphite-free C_3N_4 films were obtained under optimal conditions. The Vickers hardness of the C_3N_4 films falls in the range of 2950–5100 kgf/mm^2. The C_3N_4 films exhibit high resistance against acid and electrochemical etching. Thermal gravimetric and differential thermal analysis showed that the films are thermally stable at temperatures ranging from room temperature to 1200 °C.
[S0163-1829(97)03232-3]

I. INTRODUCTION

C_3N_4, which may have hardness greater than that of diamond, shows immense potential for applications in the field of materials science and engineering and has become an extensively studied subject in the past few years. Liu and Cohen[1,2] first predicted that the bulk modulus of the β-C_3N_4 should be 4.27 Mbar, comparable to that of diamond, which is calculated to be 4.35 Mbar and measured as 4.43 Mbar. In 1993, Niu, Lu, and Lieber[3] synthesized β-C_3N_4 from laser vaporization of high-purity graphite using a N^+ beam simultaneously bombarding the substrate. C-N films were also prepared by reactive magnetron sputtering,[4,5] ion-beam deposition,[6] electron cyclotron resonance plasma-assisted chemical vapor deposition (ECR-CVD),[7] and hot filament CVD.[8] The resulting films were predominantly amorphous. Only a few authors obtained nanometer-sized β- C_3N_4 crystallites, with a crystallization rate <5 vol. %, dispersed in the amorphous C_3N_4 matrix. On the other hand, all the C-N films reported were carbon rich. It turned out to be difficult to prepare samples with nitrogen content satisfying the C_3N_4 formula. To date, samples containing sufficient amounts of crystallized C_3N_4 and with bulk modulus comparable to the predicted value have not been obtained.

Recently, Liu and Wentzcovitch,[9] in their *ab initio* variable-cell-shape molecular-dynamics study of the C_3N_4 structure, pointed out that there exist three C_3N_4 phases: the hexagonal β-C_3N_4 (space group $P6_3/m$), the defect cubic zinc-blende ($P\overline{4}3m$) C_3N_4, and the rhombohedral C_3N_4 ($R3m$) phase, the bulk moduli of which, are 4.37, 4.25, and 0.51 Mbar, respectively. The cohesive energies of the three phases lie close to each other and are also close to those of both diamond and graphite. Hence, during the reaction process in C_3N_4 synthesis, the five phases, including diamond and graphite, will grow competitively, none of which may easily grow large. Consequently, amorphous C-N films will usually be formed. As diamond and graphite are energetically a little lower than C_3N_4, amorphous carbon should grow faster than C_3N_4.[10]

Concerning the application of C_3N_4 as coatings on cutting tools, graphite and rhombohedral C_3N_4, the two soft phases are harmful to attainment of useful mechanical properties. Restraining their growth is crucial to preparing hard C-N coatings.

This paper presents the synthesis of C_3N_4 by rf plasma-enhanced chemical vapor deposition (PECVD) and formation of large-area polycrystalline C_3N_4 films using various transition layers. The structures of the films were analyzed by x-ray diffraction (XRD) and transmission electron diffraction (TED), the nature of the C-N bonding determined by x-ray photoelectron spectroscopy (XPS) and Fourier transform infrared (FTIR) spectroscopy. The Vickers hardness of the C-N films were measured. Corrosion and thermal gravimetric and differential thermal analysis (TG-DTA) experiments were conducted to examine the chemical and thermal stability of the samples.

II. EXPERIMENTAL DETAILS

Our rf PECVD apparatus for Si_3N_4 and C_3N_4 deposition is shown in Fig. 1. The cylindrical exciting electrode of the rf power source is fitted outside the quartz tube. The substrate

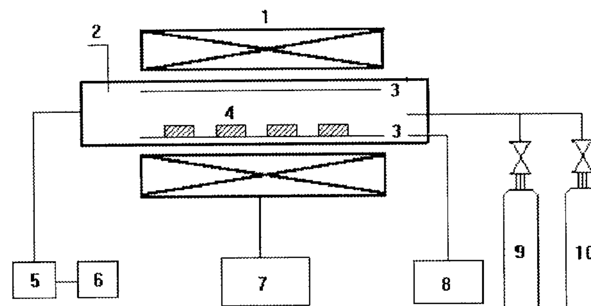

FIG. 1. A schematic diagram of the rf PECVD apparatus for the deposition of Si_3N_4 and C_3N_4. 1, Electric heater; 2, quartz tube; 3, rf exciting electrode; 4, substrate; 5, booster bump; 6, motor bump; 7, temperature monitor; 8, rf power source; 9, ethylene; 10, N_2.

0163-1829/97/56(8)/4949(6)/$10.00 © 1997 The American Physical Society

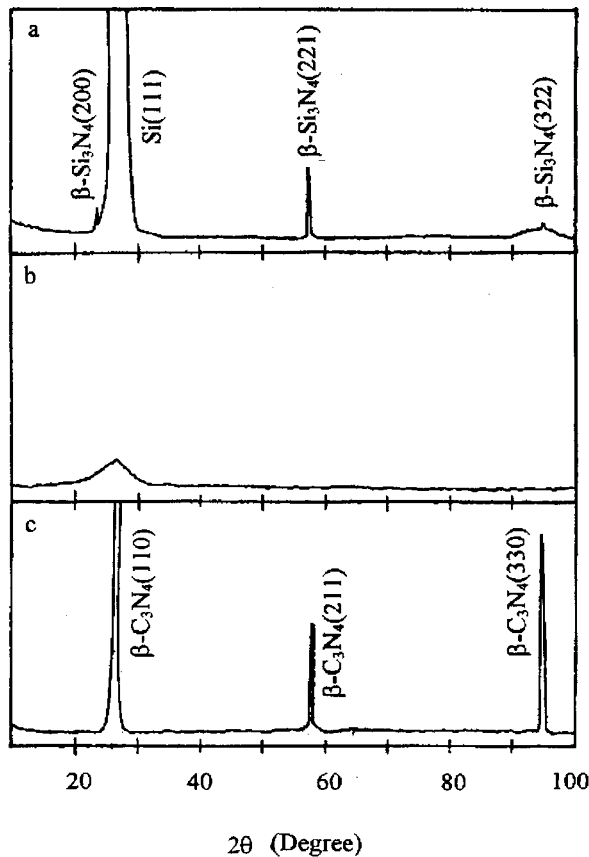

FIG. 2. The XRD spectra for Si_3N_4/Si (a), C_3N_4/Si_3N_4/Si (b), and C_3N_4/Si_3N_4/Si after annealing at 800 °C in vacuum for 2 h (c). The wide band around 28° in (b) is attributed to a scattering modification to the diffraction of β-Si_3N_4.

is placed on the grounded plate in the tube. The machine works at 200 kHz, rather than the usually adopted 13.56 MHz, and under voltages controllable between 1500–2000 V.

Polished silicon wafers were boiled first in solution NH_4OH:H_2O_2:H_2O=1:1:8 for 3 min and then in solution HCl: H_2O_2:H_2O=1:1:8 for 8 min. Then they were rinsed in hot and cold deionized water and dried up in an ir oven. A TiN or ZrN layer, 0.3–0.5 μm thick, was deposited on each wafer by reactive magnetron sputtering, followed by Si_3N_4 deposition in the PECVD chamber and then deposition of C_3N_4 films, their thickness varied to meet the requirements of various measurements. The substrate temperature was adjusted between 400–600 °C. For Si_3N_4 deposition we used SiH_4 and N_2 at fluxes of 1.3 and 3.5 liter/min, respectively, the rf voltage was controlled at 1500 V. C_3N_4 deposition was conducted at 1800 V using C_2H_4 and N_2 at 0.4 liter/min and up to 5.0 liter/min.

III. RESULTS AND DISCUSSION

A. XRD and TED analysis

To make crystalline C_3N_4, we have studied the effects of the rf power frequencies as well as transition layers on the film qualities. We believe that a low frequency favors the increase in the kinetic energy of the reactants and crystallization during deposition. A higher density of power enhances ionization and decomposition of reactants and production of carbon nitrides. And, Si_3N_4 is an ideal structural template to seed the growth of the metastable β-C_3N_4. Both compounds are in the hexagonal crystallization system. Their interface has the lowest lattice mismatch.

FIG. 3. The transmission electron diffraction pattern of a C_3N_4 film deposited on Si_3N_4. The sample was annealed at 800 °C in vacuum for 2 h before TED measurement.

XRD spectra were measured for C_3N_4/C_3N_4/Si samples at different stages of preparation. Typical results are presented in Fig. 2. For the Si_3N_4/Si sample, we see diffraction due to β-Si_3N_4(200), (221), and (322) at 2θ=26.8°, 58.9°, and 94.9°, respectively. After deposition of C_3N_4, these peaks disappear, leaving a contour around 28°, attributed to a scattering modification to the above diffraction by the freshly grown amorphous C_3N_4. For the same specimen, after annealing at 800 °C in a vacuum for 2 h, we see three peaks at 28.4°, 58.7°, and 94.9°, attributed, respectively, to β-C_3N_4(110), (211), and (330). The large intensity at 28.4° suggests a preferred growth of β-C_3N_4(110) with little lattice mismatch over β-Si_3N_4. In addition to the above three planes, there are also crystallites grown along the β-Si_3N_4(221) and (322) textures, but they are not so intense. In the above experiment, no diffraction due to graphite was observed. This is because graphite and Si_3N_4 have large mismatches, though they are in the same crystallization system. Based on the XRD spectra, the β-C_3N_4 lattice constants were

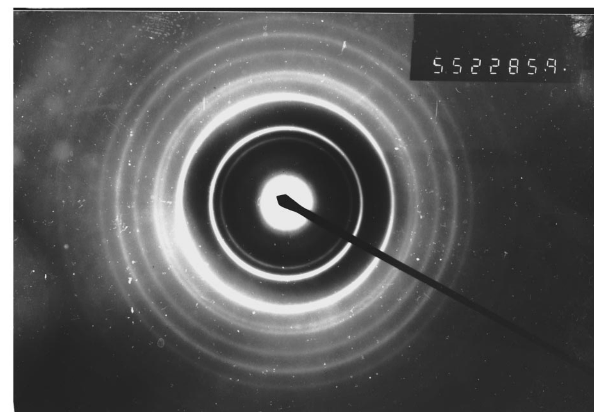

FIG. 4. The transmission electron diffraction pattern typical of C_3N_4 films deposited on Si_3N_4/TiN/Si.

TABLE I. Crystal parameters of C_3N_4 deposited on Si_3N_4/TiN/Si and Si_3N_4/ZrN/Si.

Theoretical		Experimental		Theoretical		Experimental	
(hkl)	d (Å)	C_3N_4/Si_3N_4/TiN/Si	C_3N_4/Si_3N_4/ZrN/Si	(hkl)	d (Å)	C_3N_4/Si_3N_4/TiN/Si	C_3N_4/Si_3N_4/ZrN/Si
110	3.213	3.48	3.25	321	1.133		1.13
200	2.783	2.56		500	1.106	1.11	
101	2.259	2.21		330	1.071	1.00	
111	1.953		1.95			0.90	
211	1.598	1.57	1.57			0.85	
221	1.345	1.35		611	0.80	0.79	
320	1.277	1.27	1.27			0.75	

calculated as $a=6.28$ Å and $c=2.34$ Å, in good agreement with predictions of Yu *et al.*,[11] though with slight deviations of -2.5% and -1.6%, respectively, compared to those reported in Ref. 2, and of -2.0% and 1.3% compared to those in Ref. 9.

Free C_3N_4 films were obtained by dissolution of Si, Si_3N_4, and TiN or ZrN in corrosive solution $HF:HNO_3=2:1$. TEM observation revealed that C_3N_4 films deposited on Si_3N_4/Si are amorphous. We annealed the C_3N_4/Si_3N_4/Si samples at 800 °C in a vacuum for 2 h before putting them into the corrosive solution to strip the C_3N_4 films off the substrates. Then Laue's diffraction patterns were observed for the free C_3N_4 specimens (Fig. 3), indicative again of an amorphous to crystalline C_3N_4 transition during annealing.

C_3N_4 films deposited on Si_3N_4/TiN/Si and Si_3N_4/ZrN/Si are polycrystalline, as shown in Fig. 4 for the TED pattern of a C_3N_4/Si_3N_4/TiN/Si specimen. Crystal parameters calculated from the TED patterns are summarized in Table I from which we see that the C_3N_4 films deposited on both Si_3N_4/TiN/Si and Si_3N_4/ZrN/Si are structurally analogous to β-C_3N_4, with C_3N_4/Si_3N_4/ZrN/Si even closer to it. And we also observed Laue's patterns for as-prepared C_3N_4/Si_3N_4/ZrN/Si under appropriate deposition conditions, revealing that large C_3N_4 crystallites have been formed when ZrN intermediate layers were used.

The consistency between our XRD and TED spectra have verified the existence of crystalline C_3N_4. The TED results suggest that TiN and ZrN layers enhance C_3N_4 growth over Si_3N_4. But its explanation remains a question. Our previous study showed that TiN and ZrN layers deposited on Si are crystalline.[12] Since the synthesized β-Si_3N_4 is hexagonal, the forced crystallization mechanism suggesting that the cubic TiN or ZrN layer forces its seeded layer to adopt the same cubic structure is not applicable here.[13] It may be reasonable to take account of the hexagonal symmetry nature of some TiN or ZrN planes.[14] That symmetry should result in better crystallized β-Si_3N_4 which then would better seed growth of β-C_3N_4. Further research is still under way.

B. XPS and FTIR analysis

XPS spectra of C($1s$) and N($1s$) electrons were measured and simulated, and two groups of peaks (Table II) were obtained. One is the group of carbon peaks: $C^1=286.2$–287.1 eV, $C^2=284.6$–284.8 eV; the other is the nitrogen group: $N^1=398.0$–398.7 eV, $N^2=400.3$–400.9 eV. The values were found influenced by the N_2 flux.

The results show that both sp^3 and sp^2 hybridization exist in the C-N films. In either cubic or β phase C_3N_4, each C atom is sp^3 hybridized and σ-bonded with four N atoms, forming a tetrahedral configuration. As nitrogen has a greater electronic affinity, the electron cloud of the C-N covalent bond tends to move near the N atom. This transfer of negative charge increases the binding energy of the C($1s$) and reduces the binding energy of the N($1s$) electron (compared with that of the N_2 molecule). In rhombohedral C_3N_4, each carbon atom is sp^2 hybridized and σ-bonded with three nitrogen atoms, making up a hexagonal structure. In the planar network of the hexagonal lattice, each atom, carbon or nitrogen, has a solitary electron, which forms the π bonding between the interplanar C and N atoms (C═N bonds), making the structure a stable one similar to the benzene structure frequently found in organic compounds. Owing to the presence of the C═N bonds, the rhombohedral C_3N_4 has the greatest chemical bond energy and therefore is chemically most stable among the three C_3N_4 phases. In actual C-N films, the binding-energy variation results from variation in bond forms and lengths. The nitrogen concentration, obtained from XPS, increases with the N_2 flux. Up to 53.7 at. % concentration was obtained for films deposited at the N_2 flux of 5.0 liter/min.

To further study the C-N bonding, we performed FTIR spectroscopy on a NICOLET FTIR spectrometer. Figure 5 illustrates the FTIR spectrum for a C-N film directly deposited on Si(111). The 1260 cm^{-1} peak is attributed to the stretch vibration of C-N single bonds, the frequency of which has shifted a little towards the high frequency owing to the presence of other bonds with higher frequencies and the influence of neighbor radicals. The FTIR analysis of a variety of samples prepared by the present method showed that the wave number of C-N bond vibration falls in the

TABLE II. The binding energies of C($1s$) and N($1s$) electrons and N concentrations determined from XPS spectra of the C_3N_4 films. The sample labeled a through e were prepared at N_2 fluxes 5.0, 4.5, 4.0, 3.5, and 2.5 liter/min, respectively.

Sample	a	b	c	d	e
C^1 (eV)	287.1	286.9	286.8	286.5	286.2
N^1 (eV)	398.6	398.5	398.7	398.7	398.5
C^2 (eV)	284.7	284.8	284.7	284.7	284.6
N^2 (eV)	400.8	400.5	400.8	400.9	400.3
N content (at. %)	53.7	47.6	46.7	44.4	12.0

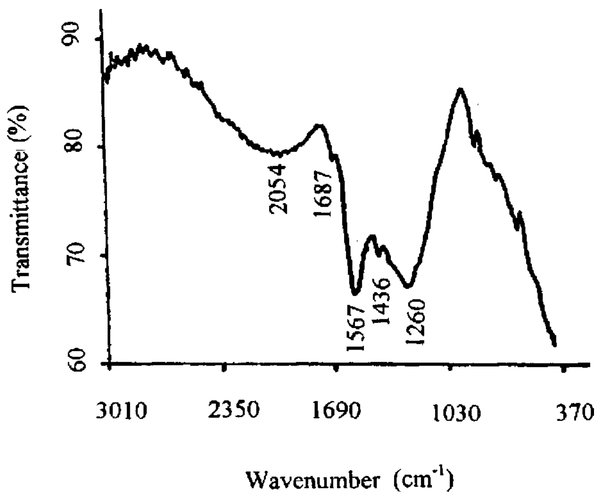

FIG. 5. The FTIR spectrum of a C_3N_4 film directly deposited on Si(111) substrate.

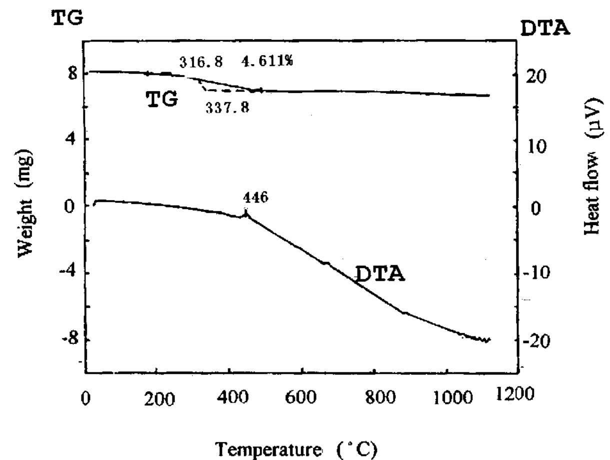

FIG. 7. The TG-DTA curves of a C-N film deposited on Si(111) substrate (sample A).

912–1062 cm^{-1} range. The 1436 cm^{-1} peak is attributed to amorphous sp^3 C-C bonds, the strong peak at 1576 cm^{-1} to the absorption of graphite, and the 1687 cm^{-1} peak to the vibration of C=N bonds, indicative of the presence of rhombohedral C_3N_4. The wide band around 2054 cm^{-1} is assigned to the C≡C bonds.

Using transition layers, we have obtained pure C_3N_4 films under optimal conditions. An FTIR spectrum typical of such films on Si_3N_4/ZrN/Si is illustrated in Fig. 6. One sees only a broad and strong absorption band around 974 cm^{-1} attributed to C-N bonds, which is much different from the spectrum shown in Fig. 5, and a peak at 614 cm^{-1} caused by lattice vibration of the Si substrate. No evidence for the presence of absorption due to graphite, expected around 1550 cm^{-1}, or any other bonds or radicals, was found.

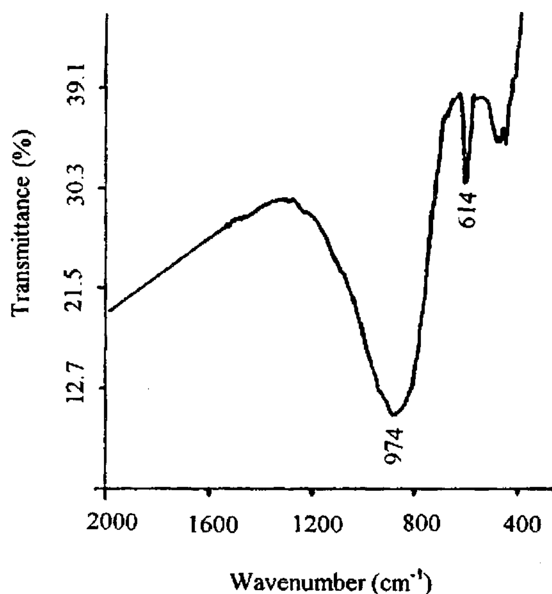

FIG. 6. The FTIR spectrum of a C_3N_4 film deposited on Si_3N_4/ZrN/Si.

C. Hardness, chemical and thermal stability

The hardness of C_3N_4 is a key parameter as far as its practical application is concerned. Our hardness measurement, conducted with a Vickers hardness tester under loads of 5 and 10 g, shows that the hardness of the C_3N_4/Si_3N_4/TiN/Si falls in the range of 3000–5100 kgf/mm^2. C_3N_4 films deposited on TiN/metal have comparatively lower hardness (3000–3300 kgf/mm^2). Here, the metal is an oil pipe alloy steel. We see that the adoption of Si_3N_4/TiN transition layers to restrain graphitic growth is successful and results in attainment of C_3N_4 films with expected high hardness.

To study the resistance of C_3N_4 against acids, we put C_3N_4/TiN/Si samples in 49 % HF acid. As TiN and Si_3N_4 dissolve easily in HF acid, the C_3N_4 film was stripped off the substrate. It was not decomposed or damaged by the acid. C_3N_4/Si samples were put in a mixture of HF and nitric acids with HF:HNO_3=2:1. The Si wafer reacted swiftly with the mixture, dissolved, and completely vanished, but the C_3N_4 films remained intact.

The resistance of C_3N_4 against electrochemical etching was studied using a solution of 10% H_2SO_4 and 10% NaCl.

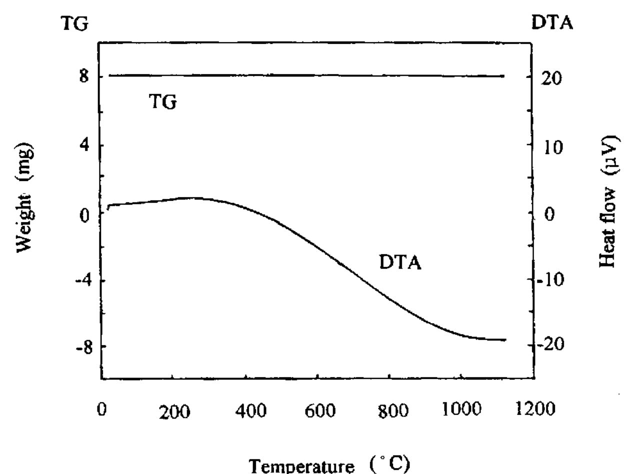

FIG. 8. The TG-DTA curves for the C_3N_4 film deposited on Si_3N_4 (sample B).

TABLE III. The electrochemical etching current and current ratio of specific electrodes under various voltages.

Working voltage (mV)	Sample	Etching current (mA/cm^2)	Current ratio	
	metal	50.0	769	3.3
−600	Cr/metal	15.0	231	1
	C_3N_4/metal	6.5×10^{-2}	1	
	metal	70.0	212	4.4
0	Cr/metal	16.0	49	1
	C_3N_4/metal	33.0×10^{-2}	1	
	metal	77.5	258	2.6
+300	Cr/metal	30.0	100	1
	C_3N_4/metal	30.0×10^{-2}	1	
	metal	210.0	575	6.7
+600	Cr/metal	31.5	86	1
	C_3N_4/metal	36.5×10^{-2}	1	
	metal	237.5	617	7.4
+800	Cr/metal	32.0	83	1
	C_3N_4/metal	38.5×10^{-2}	1	
	metal	235.0	573	7.2
+1000	Cr/metal	32.5	79	1
	C_3N_4/metal	41.0×10^{-2}	1	

Plates of oil pipe alloy steel, Cr/metal, and C_3N_4/metal, each with a conducting area of 1 cm^2, were used as working electrode. Platinum was used as pair electrode and standard calomel electrode saturated mercurous chloride as reference electrode. The results are listed in Table III and analyzed as follows.

In electrochemical etching of metals, atoms of the metal, the anode, lose their electrons and become ions dissolving in the corrosive medium. When an insulating C_3N_4 film is deposited on the surface of the metallic anode, the reaction process in which the anode is involved is greatly slowed down and the etching rate of the anode is remarkably reduced. From Table III one sees that, when C_3N_4/metal is used as an anode, the etching current decreases by 258 to 617 times compared to the case with a bare alloy metal plate as an anode and decreases by 79 to 100 times from the case where the alloy is coated with Cr.

TG-DTA was conducted for samples (designated *A* and *B*) prepared under different conditions. Sample *A* is a C-N film directly deposited on Si(111) and electrically conducting for the existence of graphite in it. On its TG curve in Fig. 7, we see a peak with a weight losing rate of 4.611% in the 316.8–337.9 °C range. Correspondingly, a heat releasing peak manifests itself on the DTA curve. It is suggested that, when heated, the graphite in the C–N film reacts with oxygen in the air, producing CO_2 gas and releasing heat, and the film loses its weight.

Sample *B* is a C-N film deposited on Si_3N_4/Si. Containing no graphite, the sample is electrically insulating. . In this case (Fig. 8), no TG peak can be observed in the temperature range from room temperature (RT) to 1200 °C. Nor does one see apparent heat releasing or gaining on the DTA curve. The C_3N_4 films prepared using Si_3N_4 buffer layers are therefore thermally stable.

IV. CONCLUSION

Polycrystalline C_3N_4 films were prepared by rf PECVD under an ethylene and nitrogen ambient using Si as substrate and Si_3N_4/TiN and Si_3N_4/ZrN as transition layers. Laue's spots were observed for C_3N_4/Si_3N_4/ZrN/Si and annealed C_3N_4/Si_3N_4/Si samples. Both sp^3 and sp^2 hybridization exist in the films. The Si_3N_4 layer is indispensable for making graphite-free C_3N_4 films. Intermediate TiN and ZrN layers enhance growth of polycrystalline C_3N_4 films over Si_3N_4 buffer layers. The nitrogen concentration of the films falls in the range of 12.0–53.7 at. %.

The Vickers hardness of the C_3N_4 films falls between 3000–5100 kgf/mm^2. The C_3N_4 films remain intact in HF acid, in mixture of HF and nitric acids, and are resistant to electrochemical etching. TG-DTA studies showed that the films are thermally stable at temperatures ranging from RT to 1200 °C.

ACKNOWLEDGMENTS

This work was supported by the National Natural Science Foundation of China. The authors thank Professor Shi Weidong of the China National Laboratory of Ion, Electron, and Photon Beams, Dalian University, for his kind help in the Vickers hardness measurement.

[1] A. Y. Liu and M. L. ohen, Science **245**, 841 (1989).
[2] A. Y. Liu and M. L. Cohen, Phys. Rev. B **41**, 10 727 (1990).
[3] C. Niu, Y. Z. Lu, and C. M. Lieber, Science **261**, 334 (1993).
[4] C. J. Torng, J. M. Sivertsen, J. H. Judy, and C. Chang, J. Mater. Res. **5**, 2490 (1990).
[5] M. Y. Chen, D. Li, X. Lin, V. P. Dravid, Y. W. Chung, and M. S. Wong, J. Vac. Sci. Technol. A **11**, 521 (1993).
[6] F. Fujimoto and K. Ogata, Jpn. J. Appl. Phys. **32**, L420 (1993).
[7] A. Bouseta, M. Lu, and A. Bensaoula, Appl. Phys. Lett. **65**, 696 (1994).
[8] Z. F. Zhang, Z. H. Zhou, and H. L. Li, Appl. Phys. Lett. **68**, 1 (1996).
[9] A. Y. Liu and R. M. Wentzcovitch, Phys. Rev. B **50**, 10 362 (1994).
[10] K. J. Boyd, D. Marton, S. Todorov, A. H. Al-Bayati, J. Kulik, R. A. Zuhr, and J. W. Rabalais, J. Vac. Sci. Technol. A **13**, 2110 (1995).
[11] K. M. Yu, M. L. Cohen, E. E. Haller, W. L. Hansen, A. Y. Liu, and I. C. Wu, Phys. Rev. B **49**, 5034 (1994).
[12] D. Wu, Z. Zhang, D. Fu, W. Fan, and H. Guo, Appl. Phys. A (to be published).
[13] X. Chu, M. S. Wong, W. D. Sproul, S. L. Rohde, and S. A. Barnett, J. Vac. Sci. Technol. A **10**, 1604 (1992).
[14] D. Li, X. Chu, S. C. Cheng, X. W. Lin, V. P. Dravid, Y. W. Chung, M. S. Wong, and D. Sproul, Appl. Phys. Lett. **67**, 10 203 (1995).